European Journal of Pharmaceutical Sciences 163 (2021) 105866

Contents lists available at ScienceDirect

European Journal of Pharmaceutical Sciences

journal homepage: www.elsevier.com/locate/ejps

Preparation and in-vitro evaluation of mesoporous biogenic silica nanoparticles obtained from rice and wheat husk as a biocompatible carrier for anti-cancer drug delivery

Sahar Porrang [a,b], Nader Rahemi [a,b,1,*], Soodabeh Davaran [c,d], Majid Mahdavi [e,f], Belal Hassanzadeh [g]

[a] Chemical Engineering Faculty, Sahand University of Technology, Sahand New Town, Tabriz, Iran
[b] Environmental Engineering Research Centre, Sahand University of Technology, Sahand New Town, Tabriz, Iran
[c] Department of Medical Nanotechnology, Faculty of Advanced Medical Science, Tabriz University of Medical Sciences, Tabriz, Iran
[d] Research Centre for Pharmaceutical Nanotechnology, Tabriz University of Medical Sciences, Tabriz, Iran
[e] Department of Biology, Faculty of Natural Science, University of Tabriz, Tabriz, Iran
[f] Department of Cell and Molecular Biology, Faculty of Biological Sciences, Kharazmi University, Tehran, Iran
[g] Faculty of Veterinary Medicine, University of Tabriz, Tabriz, Iran

ARTICLE INFO

Keywords:
Biosources
Rice husk
Wheat husk
Mesoporous biogenic silica nanoparticles
Anticancer drug delivery
Breast cancer cell-line

ABSTRACT

In this study, mesoporous silica nanocarriers were synthesized from natural sources such as rice and wheat husk for drug delivery application. First, the biogenic silica in cereals husk was extracted by acid leaching and then converted to sodium silicate as a silica precursor. Mesoporous silica nanoparticles were then synthesized by adding sodium silicate to the template mixture by continuous and discrete modes during the sol-gel process. The effects of natural sources type and precursor addition method on nanocarriers' morphological and physico-chemical properties were investigated by XRD, FT-IR, BET and SEM analysis. Our results showed rice husk-based spherical nanocarriers were more crystalline with slit-shaped pores, while wheat husk-based nanocarriers had been composed of spherical nanoparticles with narrow cylindrical pores. The results also showed that by adding the precursor discretely, their hydrophilicity, particle size and pore size increased compared with the continuous mode, probably due to the high initial concentration of the precursor in the reaction mixture. Doxorubicin (Dox), as a model anticancer drug was loaded into the nanocarriers, and the drug release behavior was studied at two different pH values (7.4 and 5.4). In general, the accumulated released drug at pH 5.4 was approximately twice as much as pH 7.4 due to the higher solubility of doxorubicin at acidic environment. Also, the accumulated released drug at pH 5.4 for nanocarriers which had been synthesized by discrete mode, was higher than continuous mode, due to the larger pore diameter of them. The biocompatibility and cytotoxicity of nanocarriers and Dox-loaded nanocarriers were also investigated on the HFF-2 and MCF-7 cell lines, respectively. Moreover, apoptosis, as the mechanism of cell death, was evaluated by morphological study of the MCF-7 cells. Within acceptable toxicity limits and apoptosis induction, the Dox-loaded nanocarriers, especially discrete mode synthesized nanocarriers, exhibited high-efficiency anticancer effect on the MCF-7 cell line.

1. Introduction

It is well known that cancer treatment with current clinical methods has many side effects, which results from the non-specificity of these methods. In other words, failing to distinguish healthy cells from cancerous cells can cause irreversible adverse effects. Doxorubicin, as an anticancer drug, was used to treat a wide variety of cancers (Alkreathy et al., 2019). One of the apparent side effects of this drug is heart disease (Abdullah et al., 2019). Fortunately, the new generation drug delivery systems have achieved excellent results in reducing side effects (Hossen et al., 2019; Singh et al., 2019). Nanocarriers are a main component of drug delivery systems that prevent drug leakage in normal tissues and

* Corresponding author.
E-mail address: n_rahemi@sut.ac.ir (N. Rahemi).
[1] http://www.sut.ac.ir

https://doi.org/10.1016/j.ejps.2021.105866
Received 7 February 2021; Received in revised form 24 April 2021; Accepted 26 April 2021
Available online 4 May 2021

protected them until they reach the cancer site. Mesoporous silica nanoparticles (MSNs) have unique and beneficial structural features, including high surface area, high pore volume, stable mesoporous structure, adjustable pore diameter, adjustable particle size, and simple internal and external surface functionalization (Wanyika et al., 2012; Lv et al., 2016; Hao et al., 2017; Jafari et al., 2019; Manzano and Valle-t-Regí, 2020). Due to their favorable structural and chemical properties, MSNs were used in various sciences, such as drug delivery and cancer treatment (Elbialy et al., 2020; Guo et al., 2020; Nik et al., 2020; Díaz-García et al., 2020; Lim et al., 2020; Zaharudin et al., 2020; Saini et al., 2020), adsorption of organic, inorganic, and gas compounds (Costa et al., 2020), catalyst (Isaeva et al., 2020; Haynes et al., 2020), enzyme immobilization (Venezia et al., 2020), etc.

MSNs can be synthesized from high-cost alkoxy silanes (Ke et al., 2020; Li et al., 2020; Mishra et al., 2020) or inexpensive and economical sodium silicate solutions (Chapa-González et al., 2018; Narayan et al., 2018). The main goals of drug delivery strategy are reducing side effects and cancer treatment costs using biocompatible and biodegradable nanocarriers. In order to achieve these goals; it is best to synthesize nanocarriers from natural sources. Scientists have found that cereal's husk such as rice and wheat are rich sources of silica. (Shaikh and Shaikh, 2013; Renuka et al., 2013; Espíndola-Gonzalez et al., 2010). These materials are agricultural wastes that can be used to synthesize MSNs as valuable and useful material (Kaliannan et al., 2019). During a morphological study of biogenic MSNs derived by rice husk, N.K. Renuka et al. synthesized MCM-41 and SBA-16 type of MSNs (Renuka et al., 2013). In another research, MCM-48 type MSNs are manufactured by H. T. Jang et al. from rice husk as precursors and a mixture of PLE (polyoxyethylene lauryl ether) and CTAB (cetyltrimethylammonium bromide) as surfactants. The surface of as-synthesis nanoparticles was functionalized by ATPES to create amine groups for CO2 adsorption (Jang et al., 2009). I. R. Shaikh et al. succeeded in synthesizing biogenic MSNs from wheat husk with a similar procedure. In their study, after an acid pretreatment followed by calcination, the wheat husk ash was obtained. The uniform size MCM-41 nanoparticles with a particle size in a range of 300 to 500 nm are synthesized by wheat husk ash as silica precursors and CTAB as a template (Shaikh and Shaikh, 2013). In this research, the biogenic silica nanoparticles were extracted from rice and wheat husk that mentioned as RSN and WSN. Then, the physicochemical properties, Dox loading efficiency, and drug delivery potential were analyzed in-vitro. To improve drug delivery efficiency, the mesoporous silica nanoparticles with various precursors adding methods (RMSN—C, RMSN-D, WMSN—C, and WMSN-D) were synthesized. Moreover, the effect of nanoparticles with various physicochemical properties on drug delivery potential was investigated entirely. The biocompatibility and toxicity of as-synthesized nanocarriers were studied by MTT assay on HFF-2 and MCF-7 cell lines as normal and cancerous model cells. Moreover, apoptosis as the mechanism of cell death, was evaluated by a morphological study of MCF-7 cells.

2. Materials and methods

2.1. Materials

Rice husk (RH) and wheat husk (WH) as silica bio-sources, were obtained from a rice and wheat mill in Iran. Sodium hydroxide, hydrochloric acid, sulfuric acid, and cetyl trimethyl ammonium bromide (CTAB: 99%) were purchased from Merck (Darmstadt, Germany) and used as surfactant agents. Doxorubicin hydrochloride (Dox) was bought from the Faculty of Tabriz Pharmaceuticals, Iran. The cell culture medium (RPMI-1640), fetal bovine serum (FBS), and penicillin-streptomycin were purchased from Gibco (Life Technologies, Paisley, Scotland). HFF-2 and MCF-7 cell lines were obtained from the Pasteur Institute of Iran (Tehran, Iran). The 5-diphenyl-2-H-tetrazolium bromide (MTT), Trypsin and dimethyl sulfoxide (DMSO) were purchased from Sigma-Aldrich, Chemical Co (St. Louis, MO USA).

2.2. Biogenic silica nanoparticles synthesis

RSNs and WSNs could be synthesized from rice husk and wheat husk, respectively. Initially, an acid pretreatment was performed to remove impurities. They should be boiled in 1 M hydrochloric acid for 3 h then, were washed with distilled water to remove residual acid and dried overnight at 90 °C. After that, husks were calcinated at 550 °C for 4 h by 5 °C/min heating rate, and the products were named as RSN and WSN, respectively.

2.3. Biogenic mesoporous silica nanoparticles synthesis

Sodium silicate solution (SSS) was needed as MSNs precursor and can be prepared by dissolving 1 g RSNs and WSNs in 7.04 mL of 1 M sodium hydroxide solution, individually. The mixture was heated at 80 °C and stirred vigorously until half of the initial volume evaporated. In this section, the effect of the biosource type in the final MSN properties was investigated. Therefore, all the steps described below were performed on both precursors. To create a mesoporous structure, CTAB was used as a template. 4.8 g of CTAB was utterly dissolved in 100 mL deionized water at 40 °C for 1 h. After that, the pH value of the solution was adjusted to 6.5 by 1 M sulfuric acid. To investigate the effect of precursors adding method to the reaction mixture on nanoparticles' physicochemical properties, two modes were considered. i) SSS was added drop by drop continuously to the CTAB solution at 40 °C for 2 h (RMSN—C). ii). Half of the SSS was added to the reaction mixture; after 1 h, the rest of the SSS was added in the discrete form (RMSN-D). In the end, the pH of the mixture was adjusted to 11.25 by 1 M NaOH solution and was further stirred for 1 h. The reaction product was aged at 100 °C for 24 h. The next day, the precipitated solid product filtered and washed with distilled water twice. Then it was dried at 90 °C for 12 h and finally, calcined at 500 °C for 4 h by of 5 °C /min heating rate. The obtained products were assigned as RMSNs and WMSNs based on MSN derived from the rice husk and MSN derived from the wheat husk.

2.4. Drug loading into the nanoparticles

5 mg of nanoparticles were completely dispersed in 2.5 mL doxorubicin (2 mg/mL) and 0.5 ml PBS mixture at room temperature for 24 h. The dispersion was centrifuged at 12,000 rpm for 6 min and carefully washed with distilled water to remove unloaded Dox. The amount of unloaded drug presented in the supernatant, was determined by using a UV spectrophotometer with a detection wavelength of 482 nm.

2.5. In vitro drug release

Nanoparticles loaded with doxorubicin were re-dispersed in 4 mL of PBS (pH 7.4 and 5.4). The dispersion was then transferred into a shaker incubator at the desired temperature. Then the solution was centrifuged, and the supernatant was replaced with fresh PBS at specified times. The amount of released drug was determined using a UV spectrophotometer with the detection wavelength of 482 nm.

2.6. Cell culture

Human breast cancer cells (MCF-7) and Human foreskin fibroblasts (HFF-2, normal cell) cells were maintained in RPMI 1640 medium supplemented with 10% (v/v) fetal bovine serum (FBS), penicillin (100 U/mL) in CO_2 humidified atmosphere containing 5% CO_2 at 37 °C.

2.7. The cytotoxicity assays

The cytotoxicity of nanoparticles against HFF-2 and MCF-7 cell lines and Dox-loaded nanoparticles against MCF-7 cells were determined by standard MTT assay. Briefly, the cells were seeded onto 96-well plates at a density of 10,000 viable cells per well and incubated for 24 h. Then the

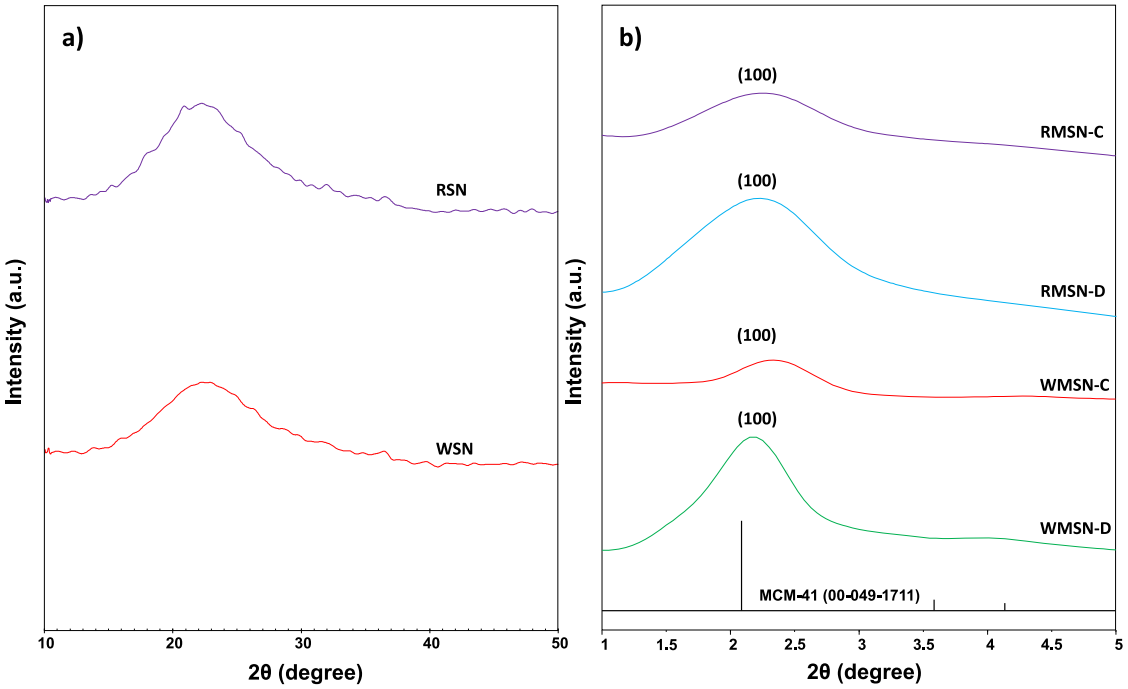

Fig. 1. X-Ray diffraction patterns of the silica nanoparticles: (a) RSN, WSN and (b) RMSN-C, RMSN-D, WMSN-C, WMSN-D.

cells were treated with Dox-loaded nanoparticles with the Dox concentrations ranging from 0.08 to 20 mg mL^{-1}, and blank nanoparticles 0.4 to 200 mg mL^{-1}, respectively, in a final volume of 200 μL. After treatment, 20 μL of MTT (5 mg/mL in PBS) was replaced in each well and incubated for an additional 3 h. Upon removing the MTT solution, the purple formazan crystals were dissolved with 100 μL DMSO, and the absorbance was recorded at 570 nm with a multi-well plate reader. Untreated cells in the medium were used as a control. All experiments were carried out with four replicates (Hu et al., 2013).

2.8. Morphological evaluation of the apoptotic cells

For morphological studies of the MCF-7 cell line, the cells were seeded in 6-well plates at a concentration of 8 × 105 cells/well, in 2 mL of the growth medium, and incubated for 24 h to allow cell attachment. The cells were treated with free Dox, Dox-loaded RMSN-D and Dox-

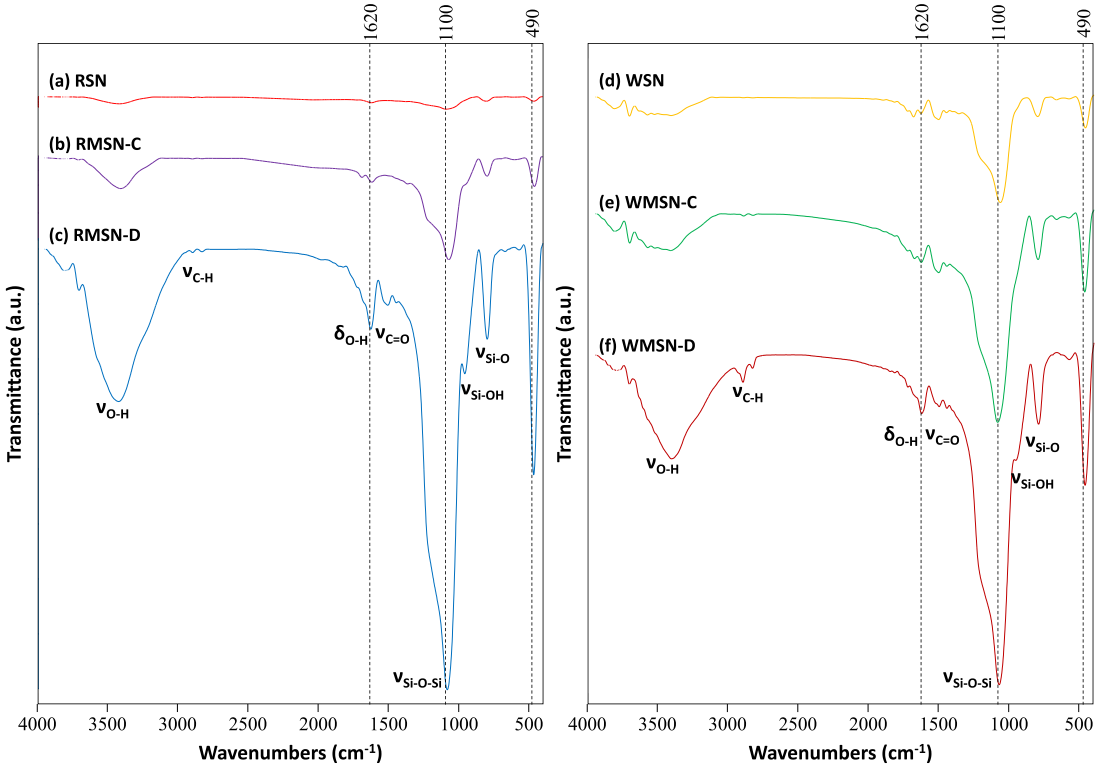

Fig. 2. FT-IR spectra of (a) RSN (b) RMSN-C (c) RMSN-D (d) WSN (e) WMSN-C (f) WMSN-D.

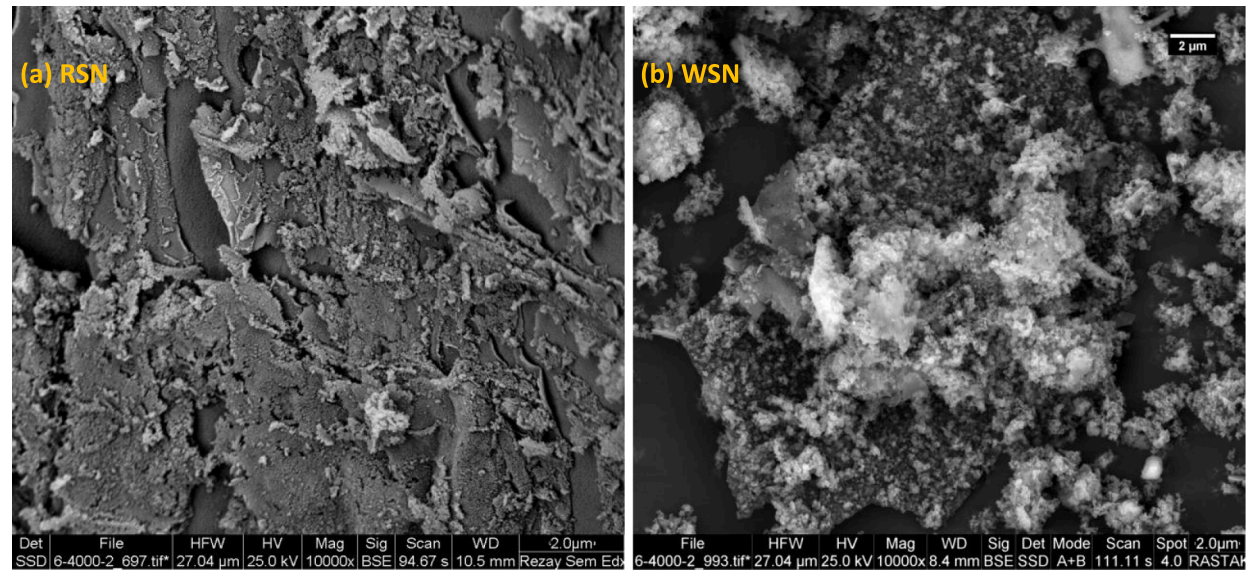

(I)

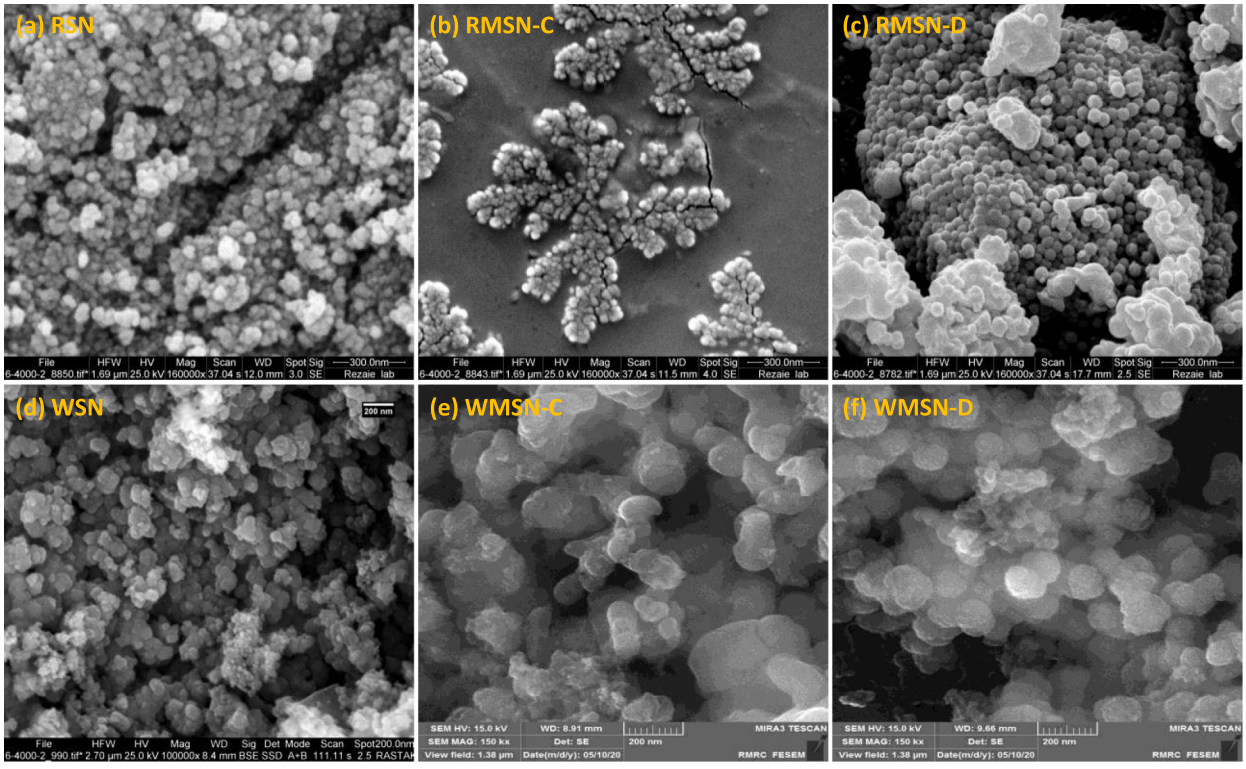

(II)

Fig. 3. SEM images of (a) RSN and (b) WSN in micro-scale (I) and (a) RSN (b) RMSN-C (c) RMSN-D (d) WSN (e) WMSN-C, and (f) WMSN-D in nano-scale (II).

loaded RMSN-D with IC 50 values obtained by MTT assay. After 48 h of incubation, DNA was also stained with Hoechst 33,258 (1 mg/mL in PBS) for 2 min, then examined using a fluorescence microscope (Aryapour et al., 2012).

3. Characterization

The low angle X-ray diffractometer (XRD) patterns of nanoparticles were recorded using a powder X-ray diffractometer (D8 Advance, Bruker AXS, Germany) with the scattering angle (2Θ) range of 10–80° for the RSN and WSN, and 1−10° for the RMSN-C, RMSN-D, WMSN-C, and WMSN-D. Fourier transform infrared (FT-IR) spectra were recorded using the FT-IR spectrophotometer (TENSOR 27, Bruker, Germany). Scanning electron microscopy (SEM) (TESCAN Vega 3, Kohoutovice, Czech Republic) images were taken with an energy-dispersive X-ray spectrum (EDS). N2 adsorption-desorption isotherms and parameters such as surface area, pore size, and pore volume were obtained with Surface Area and Pore Size Distribution Analyzer (Belsorp mini, japan).

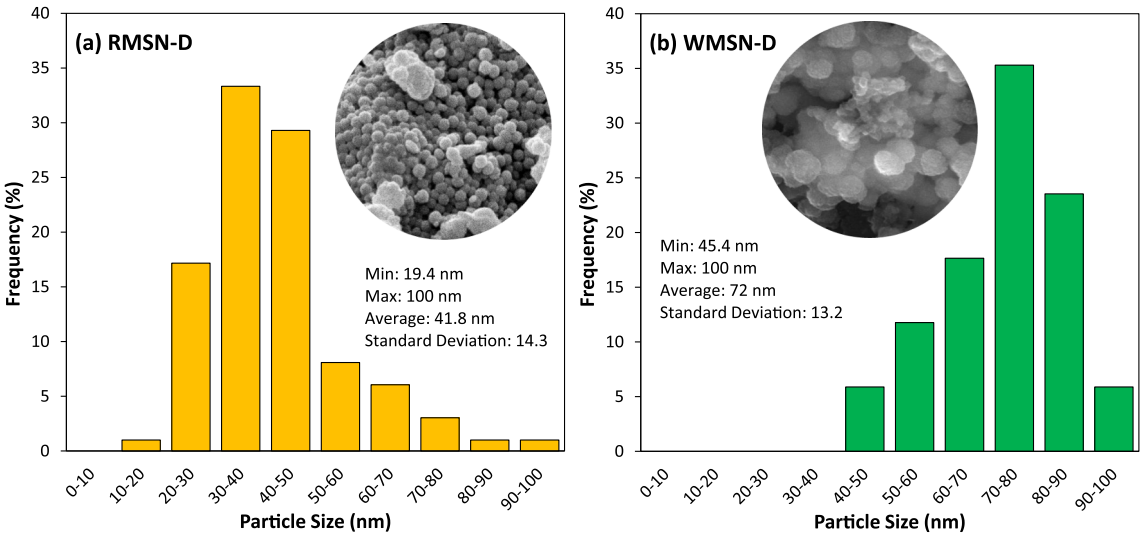

Fig. 4. Particle size distribution of RMSN-D and WMSN-D.

4. Results and discussion

4.1. Characterization

4.1.1. XRD pattern

For the synthesis of MSNs from biogenic sources, amorphous biogenic silica nanoparticles were first synthesized from rice husk as a precursor for the sol-gel process. Fig. 1-a illustrates RSN's and WSN's wide-angle XRD pattern, which appears as a broad peak at a 2θ angle of 22.17°, indicating the amorphous nature of silica. Also, no impurities were observed in the profile. Moreover, the intensity of the XRD pattern at a 2θ angle of 22.17° in RSN was higher than WSN. This result can be due to the regular structure of the rice husk compared with the wheat husk. Fig. 1-b shows low angle XRD patterns of RMSN-C, RMSN-D, WMSN-C, and WMSN-D from top to down, respectively. The XRD patterns show the crystalline state of silica with an intense peak at 2θ = 2.36° related to the reflection line (100) for all samples, which characteristic of the hexagonal structure of the mesoporous silica nanoparticles with high crystallinity (La-Salvia et al., 2017).

As shown in Fig. 1-b, RMSN-C and RMSN-D had a bit higher intensity at 2θ = 2.36° than WMSN-C and WMSN-D, which was related to the property of the bio-sources. Also, MSNs, which synthesized by discrete SSS adding mode (RMSN-D & WMSN-D), are more crystalline than continuous precursor adding mode (RMSN-C & WMSN-C). This significant change in intensity could be due to the lack of necessary time for crystals to grow in continuously precursor adding methods. This parameter can influence the nanocarrier's drug loading efficiency and release behavior.

4.1.2. FT-IR detection

The infrared spectrum of absorption or emission of RSN, RMSN-C, RMSN-D, WSN, WMSN-C, and WMSN-D were obtained by Fourier-transform infrared spectroscopy (FTIR) technique which illustrated in Fig. 2. The characteristic bands of silica nanoparticles are visible at 460, 810, and 1100 cm^{-1} due to Si–O–Si bending vibration, Si–O–Si symmetric stretching and Si–O–Si asymmetric vibration (Beygi et al., 2016) in all samples that allow identifying the SiO_2 networks. The peak at 3450 cm^{-1} was related to symmetric stretching of the Si-OH group, and the O—H stretching vibration of H_2O was visible at 1620 cm^{-1} and 950 cm^{-1} (Xu et al., 2015; Lenza and Vasconcelos, 2001). These findings indicated that silica networks of particles were successfully obtained in all the samples. The peak at 3920 cm^{-1} was related to the C—H band due to residual CTAB in samples. However, by discrete form synthesis nanoparticles (RMSN-D and WMSN-D), the characteristic bands of silica and the peaks located at 950, 1620, and 3450 cm^{-1} are stronger. This allows us to assuming that, by synthesizing mesoporous silica nanoparticles with discrete precursor adding method, a denser silica network was formed. Moreover, RMSN-D and WMSN-D are further hydrated than RMSN-C and WMSN-C (Espíndola-Gonzalez et al., 2010). This property improvement is significant because the organic moieties could attach to inorganic Si using silanol groups. So, drug delivery potential improved by developing functionalized mesoporous silica nanoparticles and targeted drug delivery systems.

4.1.3. SEM observation

The morphological properties and the size of nanoparticles were analyzed by scanning electron microscope (SEM). Fig. 3-i, illustrated the micro-scale of RSN and WSN. The RSN nanoparticles had a regular structure compared to WSN. However, WSN nanoparticles had microchannels in their structure which can affect their drug delivery properties. As illustrated in Fig. 3-ii, RSN, RMSN-C, RMSN-D, WSN, WMSN-C, and WMSN-D are spherical in nano-scale. It is evident that, by synthesizing RMSNs and WMSNs from RSNs and WSNs, the boundary between nanoparticles has become explicit, and the uniform nanoparticles were synthesized. The average hydrodynamic diameter of the nanoparticles of RSN, RMSN-C, RMSN-D, WSN, and WMSN-C was 28.76, 32.46, 41.8, 49.18, 63, and 72 nm, respectively. So, the particle size of RMSN-D and WMSN-D was increased compared with RMSN-C and WMSN-C. This phenomenon can be explained by silica precursor concentration at the beginning of the reaction. In the RMSN-D and WMSN-D cases, the higher sodium silicate solution was added compared to RMSN-C and WMSN-C at the beginning of the sol-gel process. Also, increasing the silica precursor ratio to water can cause an increase in particle size because it encourages hydrolysis and condensation reactions (Dabbaghian et al.,

Table 1
Elemental Analysis for samples.

Elements (W %)	RSN	RMSN-C	RMSN-D	WSN	WMSN-C	WMSN-D
Si	63.76	59.17	71.02	49.64	57.86	70.91
O	36.24	40.83	28.98	50.36	42.14	29.09

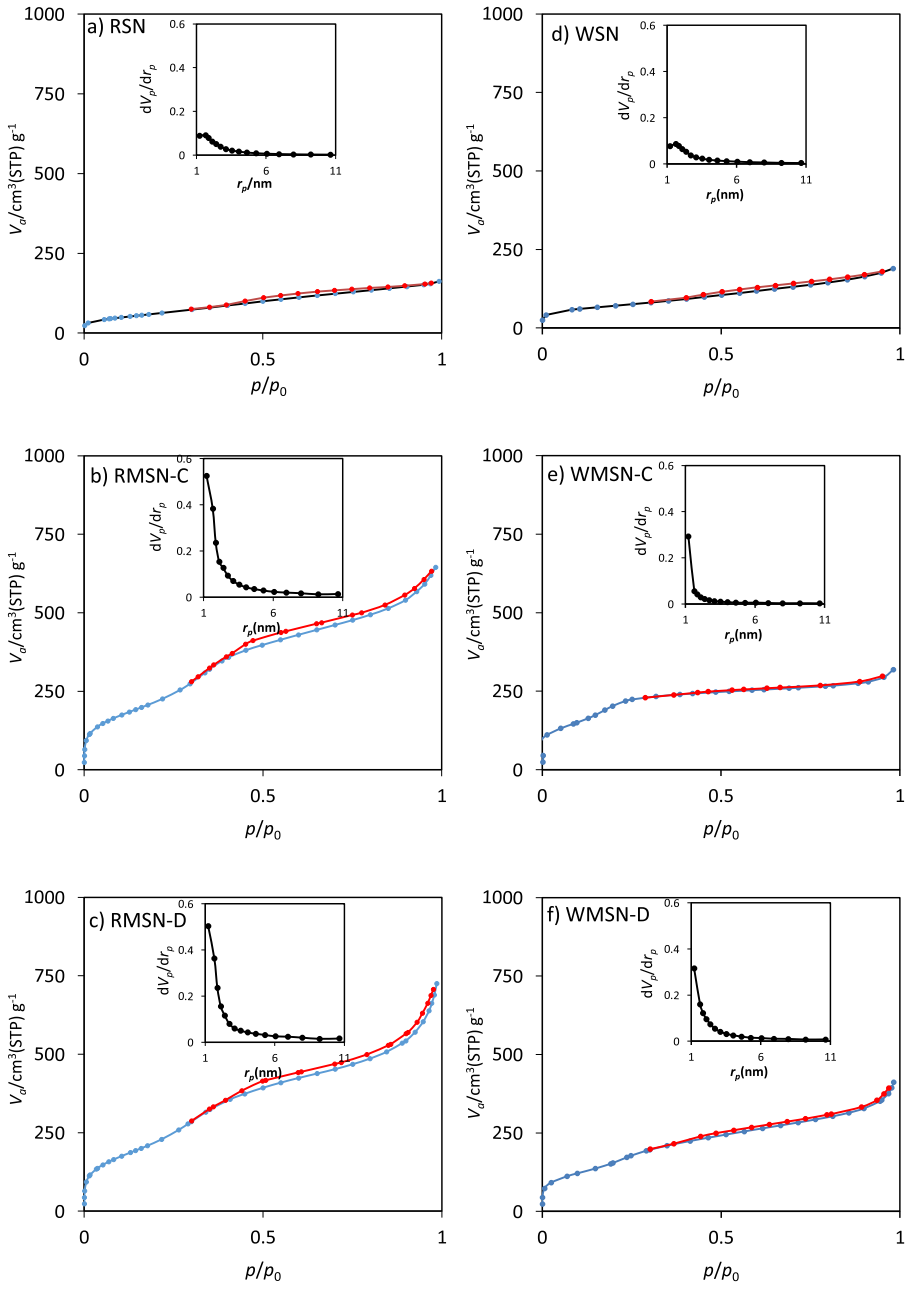

Fig. 5. The N_2 adsorption–desorption isotherm and BJH pore diameter distribution of (a) RSN (b) RMSN-C (c) RMSN-D (d) WSN (e) WMSN-C (f) WMSN-D.

2010). The particle size distribution of RMSN-D and WMSN-D was illustrated in Fig. 4.

The elemental analysis was determined by Energy-dispersive X-ray spectroscopy (EDS). Table 1 proposed a mass percentage of elements in nanoparticles. All the samples consist of Si and O elements, which indicate the silica network existence. The ratio of Si to O for RMSN-C and WMSN-C was 1.44 and 1.37. However, the ratio of Si to O for RMSN-D and WMSN-D was increased to 2.45 and 2.43, respectively.

4.1.4. *Brunauer-Emmett-Teller (BET) surface area analysis*

To improve the drug delivery capacity of RSNs and WSNs, CTAB as a template was used to create a mesoporous structure with a high specific surface area and appropriate total pore volume. These parameters are critical to increasing drug loading efficiency and encapsulation capacity. In Fig. 5, N2 adsorption/desorption isotherms for all the silica samples has been shown. Pore size distributions for these samples has been shown in the inset. According to IUPAC classification (Thommes et al.,

Table 2
Specification of the different silica nanoparticles.

Type of nanoparticles	RSN	RMSN-C	RMSN-D	WSN	WMSN-C	WMSN-D
$a_{s,BET}$ (m^2g^{-1})	226.52	969.81	950.76	242.95	841.76	617.35
Total pore volume (cm^3g^{-1})	0.2498	0.9976	1.1218	0.2924	0.4925	0.6362
Average pore diameter (nm)	4.4105	4.1144	4.717	4.146	2.3402	4.122

Table 3
Silica nanoparticles drug loading and encapsulation efficiency.

Type of nanoparticles	RSN	RMSN-C	RMSN-D	WSN	WMSN-C	WMSN-D
Loading (%)	23.33	31.34	32.19	19.14	47.52	42.06
Encapsulation (%)	19.43	26.11	26.81	15.94	39.58	35.04

2015), isotherms globally represent type IV, which confirmed the existence of mesoporous structure (Xu et al., 2015). With a more detailed investigation of charts, as illustrated in Fig. 5 (b and d), RMSN-C and RMSN-D were compatible with type IV(a) isotherm, in which pores condensation were accompanied by hysteresis type H3 at the relative pressure p/p0 = 0.4–1.0 (Sotomayor et al., 2018). This type of hysteresis belongs to the slit-like pores. On the other side, WMSN-C and WMSN-D adsorption/desorption isotherms were reversible, and they were compatible with type IV(b) isotherm, which represents narrow mesoporous (cylindrical pores less than ~4 nm for nitrogen at 77 K) (Sotomayor et al., 2018). So, the difference in the pore types of nanocarriers can influence their drug delivery potential. The corresponding pore size distribution curve indicated that the nanoparticles had a narrow pore size reported in Table 2. According to the BET results, RSNs and WSNs had a specific surface area of 226.52 and 242.95 cm^2g^{-1}, respectively. Also, the average pore volume of them was 0.2498 and 0.2924 cm^3g^{-1}. To improve physicochemical properties, RMSNs and WMSNs were synthesized based on RSNs and WSNs. RMSN-C and RMSN-D were synthesized by high specific area and very high average pore volume of 969.81, 950.76 cm^2g^{-1}, 0.9976, and 1.1218 cm^3g^{-1}, respectively. As reported in Table 2, the specific surface area and the average pore volume of WMSN-C and WMSN-D had increased compared to WSN. However, these parameters were lower than RMSN-C and RMSN-D. Due to the utterly identical synthesis method, these differences probably were due to the type of biological source. Furthermore, precursors' addition during the synthesis of MSNs in a continuous mode has raised the

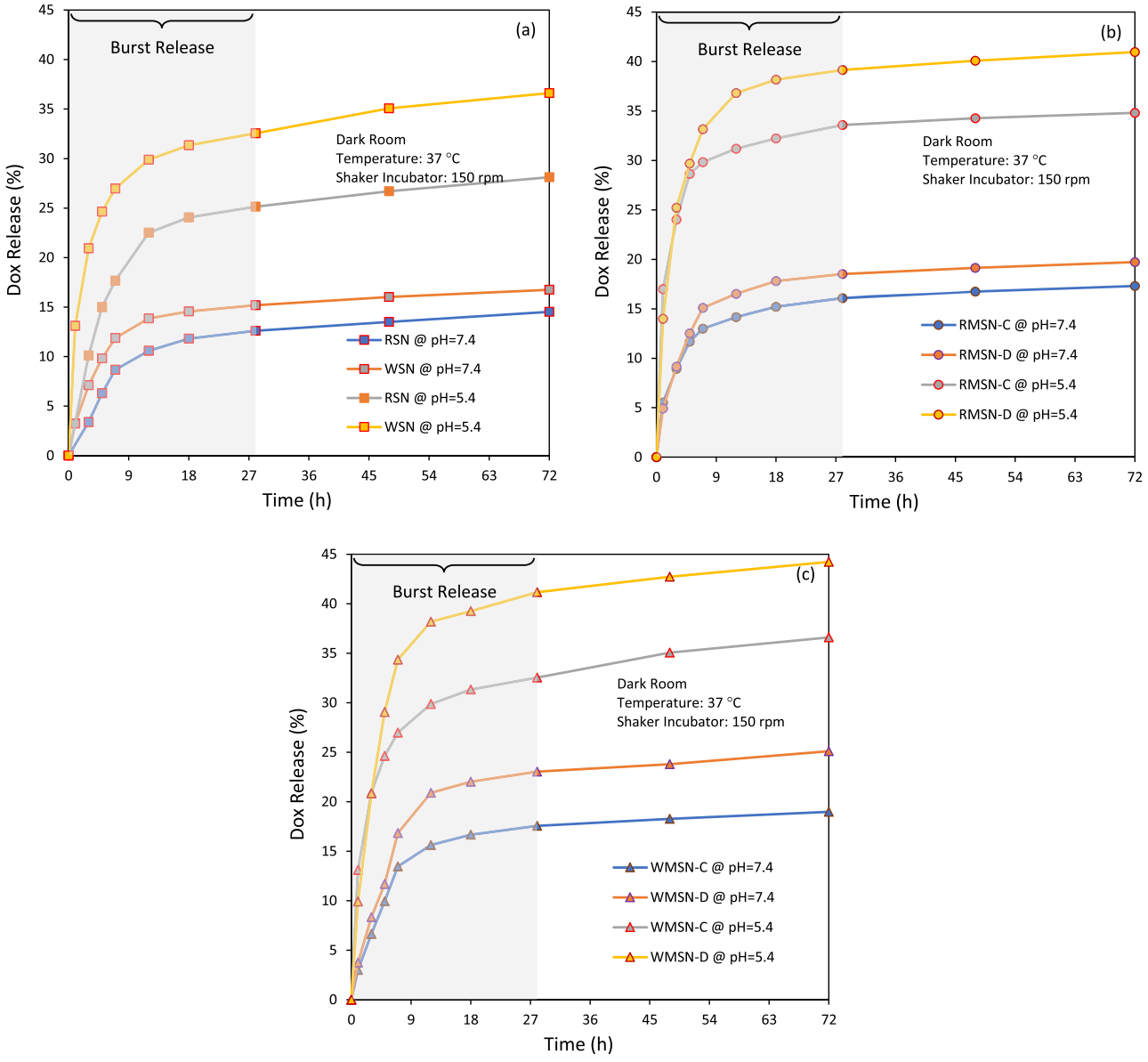

Fig. 6. Dox release profiles from (a) Dox@RSN and Dox@WSN, (b) Dox@ RMSN-C and RMSN-D (c) WMSN-C and WMSN-D nanoparticles under different pH.

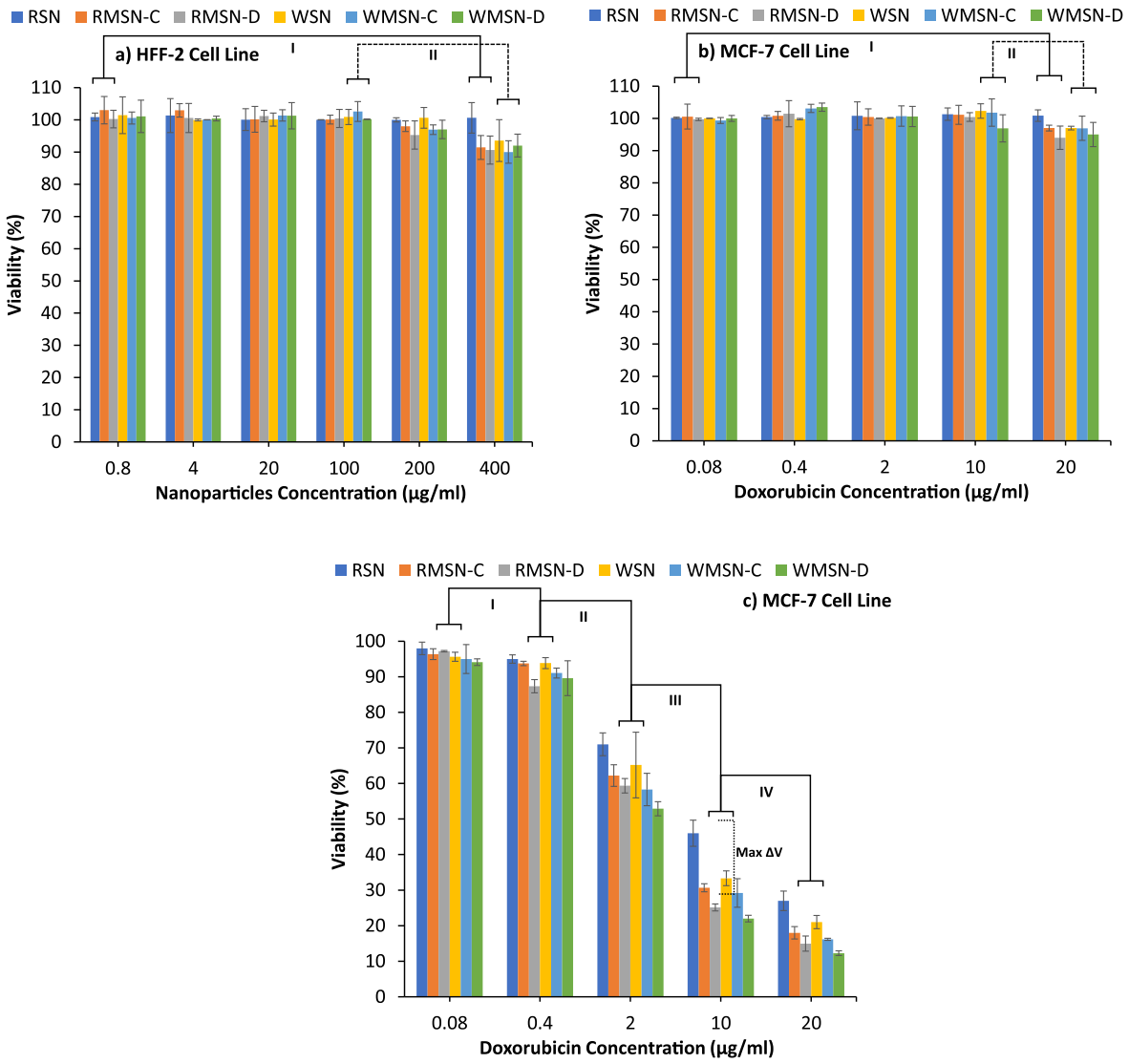

Fig. 7. The cytotoxicity and of different nanoparticles to (a) HFF-2 clells, (b) blank nanoparticles to MCF-7 cells and (c) Dox added nanoparticles to MCF-7 cells.

specific surface area. On the other side, discrete mode has created nanoparticles with a higher average pore volume and larger pore diameter. All these parameters are critical in the drug delivery field and nanocarriers efficiency.

4.2. *In-vitro pH-responsive drug release*

Dox as an anti-cancer drug with pH-dependent hydrophilicity (Kamba et al., 2013) was loaded into the nanoparticles via a simple mixture method at room temperature. The unloaded Dox was removed by centrifugation, and the loading efficiency was calculated by measuring the concentration of the unloaded drug using UV–Vis spectra. The Dox loading percentage and encapsulation efficiency were presented in Table 3.

In this study, the main purpose of using CTAB was to improve the drug delivery efficiency of RSN and WSN nanocarriers. The specific surface area, the specific pore volume, and the average pore diameter are the effective parameters in the drug delivery applications (Bavnhøj et al., 2019). Increasing the specific surface area or equivalently reducing the specific pore volume imposed to improve the drug loading (Bavnhøj et al., 2019). However, it should be noted that, an excessive increase in the specific surface area leads to prepare nanocarriers with smaller pores diameter than model drug size, such that the drug cannot be able to penetrate the nanocarrier (Li et al., 2019). Therefore, nanocarriers must have the appropriate pore size for effective drug loading. As reported in Table 3, RMSN-C, RMSN-D, WMSN-C, and WMSN-D nanocarriers have a higher loading percentage than RSN and WSN due to the increase in their specific surface area. However, another critical point is the type of pores and their accessibility, affecting the drug loading. RMSN-C and RMSN-D nanocarriers, despite their higher specific surface area, have lower loading efficiency than WMSN-C and WMSN-D nanocarriers. The reason probably depends on the morphology of the pores. The results show that the cylindrical pores of WMSN-C and WMSN-D have a higher loading capacity than the slit-like pores of RMSN-C and RMSN-D.

The release profile of Dox from the nanocarriers was investigated at two different pH values (5.4 and 7.4), which represent the acidic tumor microenvironment and normal physiological environment, respectively, at the body temperature. In all cases, the acidic condition improved the drug release into the buffer. This pH-responsive behavior can be explained by the solubility variation of Dox at different pHs. A low pH leads to Dox hydrophilicity and solubility increasing by enhancing protonated amine groups on it, which afforded the fast drug release from the nanoparticles (Hu et al., 2015). As mentioned before, RSNs and WSNs as precursors have potential for drug delivery applications. As shown in Fig. 6(a), RSNs could release 14.5% and 28.12% of

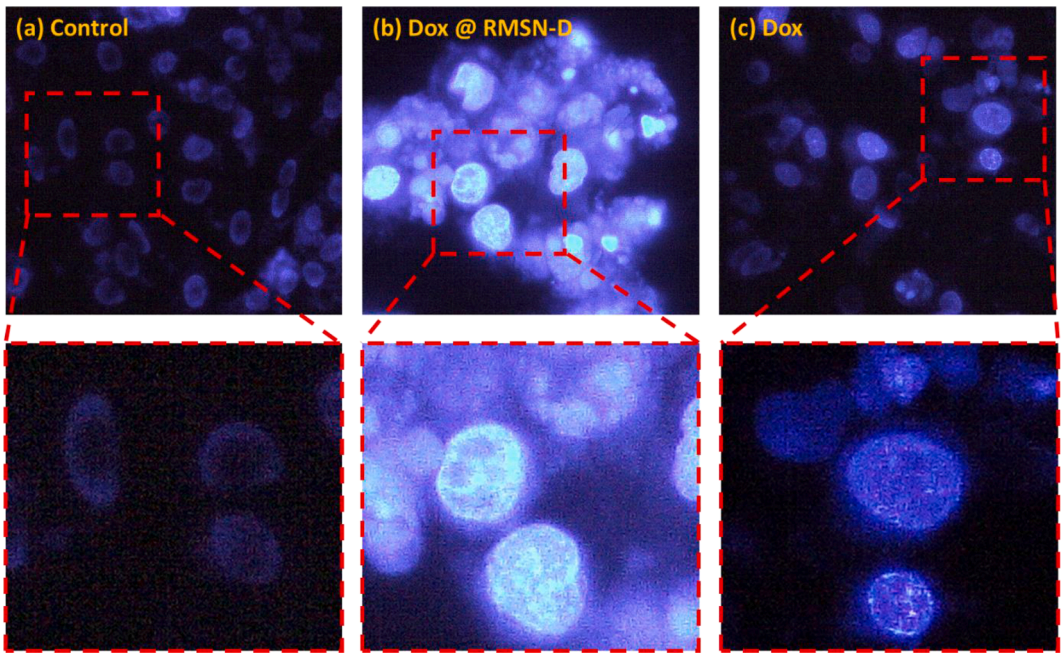

Fig. 8. Fluorescence microscopy of the MCF-7 cells (a) without treated (control) (b) treated with Dox@RMSN-D (c) Dox. Fluorescence images of the cells stained with Hoechst 33258 after 48 h. All of the investigated chromenes induced condensation and fragmentation of the nuclei.

accumulated Dox at basic and acidic conditions after 72 h, respectively. Also, WSNs can release a more significant amount of accumulated Dox (16.74% and 36.61%) under the same conditions. It can be due to a larger pore diameter of WSNs compared to RSNs (Limnell et al., 2011). RMSNs and WMSNs release patterns were illustrated in Fig. 6 (b and c). Accumulative Dox releases from WMSN were a bit higher than RMSN; however, it is noteworthy that the release pattern in wheat husk-based nanoparticles (WMSN) has a steeper slope compared to RMSN. It can be due to the higher accessibility of WMSNs pores. Moreover, as analyzed in Fig. 6 (b and c), RMSN-D, and WMSN-D, which have high crystallinity and larger pore size, have a higher accumulated amount of released Dox, compared to RMSN-C and WMSN-C with lower crystallinity at the same time. Our results indicate that using discrete methods in the precursor addition increases the drug release in the tumor medium.

4.3. MTT assay

In-vitro MTT assay was applied on human fibroblast cell line (HFF-2) for examining cytotoxicity and biocompatibility of blank nanoparticles with the nanoparticle's concentrations ranging from 0.8 to 400 μg mL^{-1}. As the results were presented in Fig. 7(a), no significant toxicity of the blank nanoparticles was observed on the normal cell line. These results show the high biocompatibility of nanocarriers. Also, the toxicity of the blank and Dox-loaded RSN, RMSN-C, WSN, RMSN-D, WMSN-C, and WMSN-D were investigated by evaluating the cytotoxicity on the MCF-7 cell line with the Dox concentration ranging from 0.08 to 20 μg mL^{-1}. As shown in Fig. 7(b), blank nanoparticles had no significant toxicity on the MCF-7 cells. However, the cytotoxicity of Dox-loaded nanoparticles was shown in Fig. 7(c). All of the nanoparticles showed acceptable toxicity on the cancerous cell lines. However,as expected the toxicity of RMSN-D and WMSN-D have been higher due to their higher drug release ability. So, these biogenic drug delivery systems by excellent biocompatibility can be high-efficiency drug delivery systems in cancer therapy.

4.4. Morphological assay of the apoptotic cells

In this section MCF-7 cells were cultured at a density of 8×10^5 cells/well in the presence of indicated concentrations (IC50 Values) of the Dox-loaded RMSN-D and Dox for 48 h. Harvested cells were stained with Hoechst 33258 to detect the apoptotic cells (Fig. 8). Under a fluorescence microscope, the control cell's nucleus was large and round, without any condensation and fragmentation. However, cells treated with Dox-loaded RMSN-D and Dox exhibited chromatin condensation and fragmentation, a typical morphological feature of apoptosis. As illustrated in Fig. 8, the chromatin condensation and fragmentation are wider in the cells treated with Dox-loaded RMSN-D. These data indicate that the investigated compounds have induced apoptosis in the MCF-7 cell line (Naseri et al., 2015).

5. Synthesis mechanism

In this study, RSN and WSN nanocarriers were extracted from rice and wheat husk by acid treatment and calcination processes. The synthesis mechanism was illustrated in Fig. 9(a). To improve physicochemical properties, loading efficiency, and encapsulation capacity, as illustrated in Fig. 9(b), sodium silicate solution as silica precursor was synthesized from RSN and WSN. Moreover, by continuous and discrete sodium silicate solution adding modes to the template mixture, RMSN-C, RMSN-D, WMSN-C, and WMSN-D nanocarriers were synthesized by sol-gel process. One of the salient features of these nanocarriers were their high specific surface area and high loading efficiency, which can induce a high potential in MCF-7 cells death.

6. Conclusion

In conclusion, we have developed novel economic biogenic mesoporous silica nanoparticles based on rice husk and wheat husk as biosources. In this paper, the effect of biosources and their adding modes to reaction mixtures for MSN synthesizing with various properties were investigated. These parameters can influence the physicochemical properties and drug delivery potential. Dox, a typical anticancer drug, was effectively loaded into the nanoparticles. The release profile of Dox from them was investigated at two different pH values 5.4 and 7.4. All of the samples have higher accumulative release behavior at the acidic condition. So, nanoparticles were pH-responsive due to highlight the

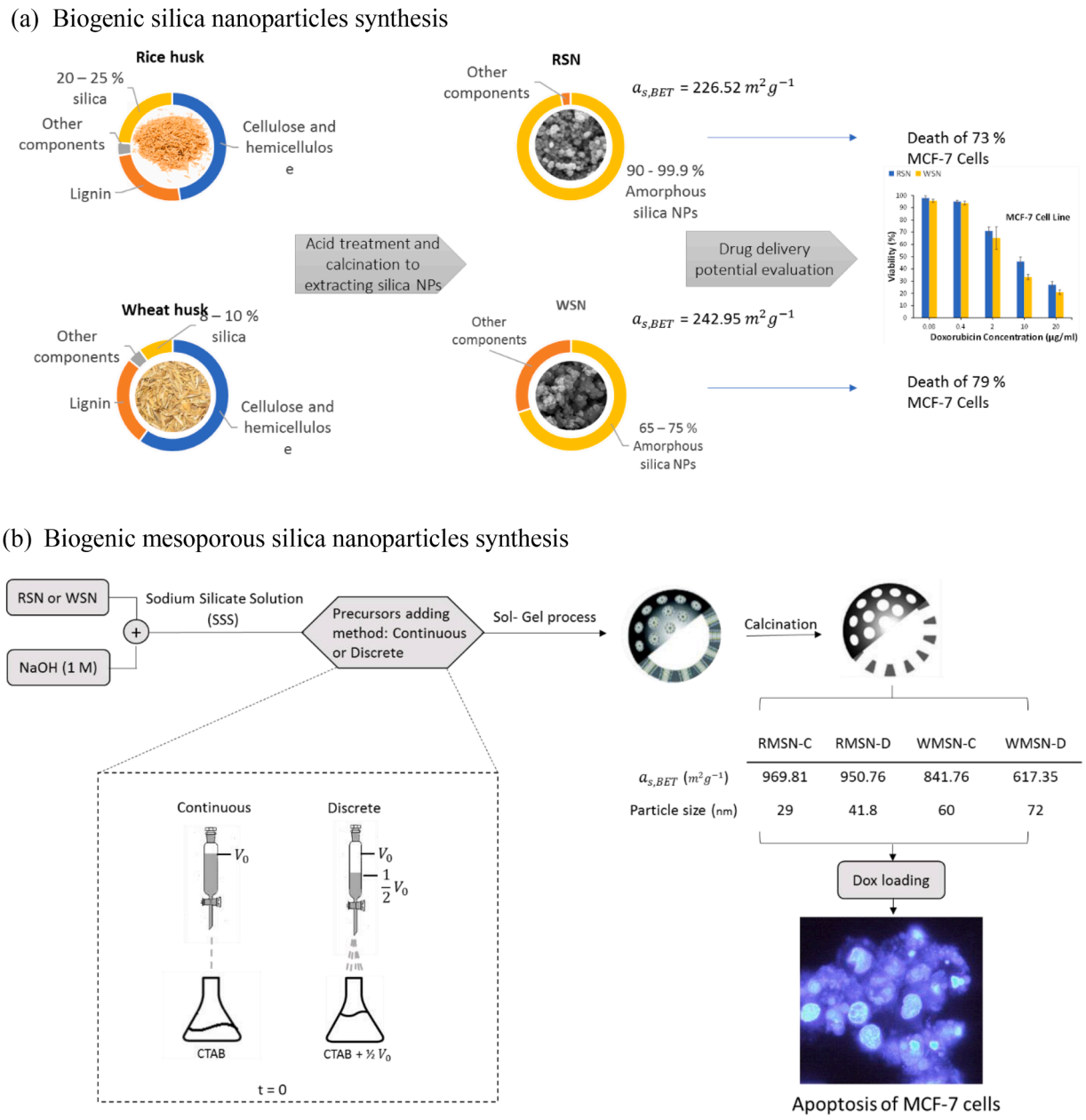

Fig. 9. Synthesis mechanism of (a) Biogenic silica nanoparticles and (b) biogenic mesoporous silica nanoparticles from rice and wheat husk by two different precursors adding methods.

Dox solubility variation in different pHs. At pH 7.4, Dox was less soluble in water and was protected in the nanoparticle's pores. By decreasing the pH to 5.4, the hydrophilicity of Dox enhanced and caused to higher release rate in acidic condition. Biogenic silica nanoparticles (RSN and WSN) have mesopores in nature which could protect the anticancer drug. To improve the drug loading capacity, RMSNs and WMSNs were synthesized by CTAB using as a template. In this way, the specific surface area was increased and led to higher Dox loading. The MSNs, which were synthesized by discrete adding precursors mode (RMSN-D and WMSN-D) had higher crystallinity and showed higher drug release rate at the acidic condition. Moreover, in this study, it was found that only a high level of specific surface area was not the reason for the high drug loading and drug release rate. The pore structure is a valid parameter in the drug loading and release profile. WMSNs had a low specific surface area than RMSNs, but they had higher drug loading and release rates. It was shown that the pore accessibility in the WMSNs was more convenient. The biocompatibility of nanoparticles was investigated by MTT assay on the HFF-2 cell line, and they have no significant toxicity. Also, the Dox-loaded nanoparticles had acceptable toxicity on the MCF-7 cells. Ultimately, the as-synthesized economic and biocompatible biogenic drug delivery systems would provide great potential for the development of cancer therapy.

CRediT authorship contribution statement

Sahar Porrang: Conceptualization, Methodology, Visualization, Investigation, Writing – original draft. **Nader Rahemi:** Supervision, Data curtion, Validation, Funding acquisition, Writing - review & editing. **Soodabeh Davaran:** Supervision, Data curtion. **Majid Mahdavi:** Supervision, Data curtion. **Belal Hassanzadeh:** Supervision, Data curtion.

Acknowledgements

The authors gratefully acknowledge Iran National Science Foundation for the financial support of the research under project number 97014149 as well as Sahand University of Technology for complementary financial supports. This work has been supported by the Iran National Science Foundation (INSF, Granted Research chair awards)

References

Alkreathy, H.M., Alkhatib, M.H., Al Musaddi, S.A., Balamash, K.S.A., Osman, N.N., Ahmad, A., 2019. Enhanced antitumour activity of doxorubicin and simvastatin combination loaded nanoemulsion treatment against a Swiss albino mouse model of Ehrlich ascites carcinoma. Clin. Exp. Pharmacol. Physiol. 46 (5), 496–505.

Abdullah, C.S., Alam, S., Aishwarya, R., Miriyala, S., Bhuiyan, M.A.N., Panchatcharam, M., Pattillo, C.B., Orr, A.W., Sadoshima, J., Hill, J.A., 2019. Doxorubicin-induced cardiomyopathy associated with inhibition of autophagic degradation process and defects in mitochondrial respiration. Sci. Rep. 9 (1), 1–20.

Hossen, S., Hossain, M.K., Basher, M., Mia, M., Rahman, M., Uddin, M.J., 2019. Smart nanocarrier-based drug delivery systems for cancer therapy and toxicity studies: a review. J. Adv. Res. 15, 1–18.

Singh, A.P., Biswas, A., Shukla, A., Maiti, P., 2019. Targeted therapy in chronic diseases using nanomaterial-based drug delivery vehicles. Signal Transduct. Targeted Therapy 4 (1), 1–21.

Wanyika, H., Gatebe, E., Kioni, P., Tang, Z., Gao, Y., 2012. Mesoporous silica nanoparticles carrier for urea: potential applications in agrochemical delivery systems. J. Nanosci. Nanotechnol. 12 (3), 2221–2228.

Lv, X., Zhang, L., Xing, F., Lin, H., 2016. Controlled synthesis of monodispersed mesoporous silica nanoparticles: particle size tuning and formation mechanism investigation. Microporous Mesoporous Mater. 225, 238–244.

Hao, N., Li, L., Tang, F., 2017. Roles of particle size, shape and surface chemistry of mesoporous silica nanomaterials on biological systems. Int. Mater. Rev. 62 (2), 57–77.

Jafari, S., Derakhshankhah, H., Alaei, L., Fattahi, A., Varnamkhasti, B.S., Saboury, A.A., 2019. Mesoporous silica nanoparticles for therapeutic/diagnostic applications. Biomed. Pharmacother. 109, 1100–1111.

Manzano, M., Vallet-Regí, M., 2020. Mesoporous silica nanoparticles for drug delivery. Adv. Funct. Mater. 30 (2), 1902634.

Elbialy, N.S., Aboushoushah, S.F., Sofi, B.F., Noorwali, A., 2020. Multifunctional curcumin-loaded mesoporous silica nanoparticles for cancer chemoprevention and therapy. Microporous Mesoporous Mater. 291, 109540.

Guo, Y., Wu, L., Gou, K., Wang, Y., Hu, B., Pang, Y., Li, S., Li, H., 2020. Functional mesoporous silica nanoparticles for delivering nimesulide with chiral recognition performance. Microporous Mesoporous Mater. 294, 109862.

Nik, A.B., Zare, H., Razavi, S.S., Mohammadi, H., Torab-Ahmadi, P., Yazdani, N., Bayandori, M., Rabiee, N., Mobarakeh, J.I., 2020. Smart drug delivery: capping strategies for mesoporous silica nanoparticles. Microporous Mesoporous Mater., 110115

Díaz-García, D., Sommerova, L., Martisova, A., Skoupilova, H., Prashar, S., Vaculovic, T., Kanicky, V., del Hierro, I., Hrstka, R., Gómez-Ruiz, S., 2020. Mesoporous silica nanoparticles functionalized with a dialkoxide diorganotin (IV) compound: in search of more selective systems against cancer cells. Microporous Mesoporous Mater., 110154

Lim, E.-B., Vy, T.A., Lee, S.-W., 2020. Comparative release kinetics of small drugs (ibuprofen and acetaminophen) from multifunctional mesoporous silica nanoparticles. J. Mater. Chem. B 8 (10), 2096–2106.

Zaharudin, N.S., Isa, E.D.M., Ahmad, H., Rahman, M.B.A., Jumbri, K., 2020. Functionalized mesoporous silica nanoparticles templated by pyridinium ionic liquid for hydrophilic and hydrophobic drug release application. J. Saudi Chem. Soc. 24 (3), 289–302.

Saini, K., Prabhuraj, R., Bandyopadhyaya, R., 2020. Development of mesoporous silica nanoparticles of tunable pore diameter for superior gemcitabine drug delivery in pancreatic cancer cells. J. Nanosci. Nanotechnol. 20 (5), 3084–3096.

Costa, J.A.S., de Jesus, R.A., Santos, D.O., Mano, J.F., Romão, L.P., Paranhos, C.M., 2020. Recent progresses in the adsorption of organic, inorganic, and gas compounds by MCM-41-based mesoporous materials. Microporous Mesoporous Mater. 291, 109698.

Isaeva, V., Chernyshev, V., Fomkin, A., Shkolin, A., Veselovsky, V., Kapustin, G., Sokolova, N., Kustov, L., 2020. Preparation of novel hybrid catalyst with an hierarchical micro-/mesoporous structure by direct growth of the HKUST-1 nanoparticles inside mesoporous silica matrix (MMS). Microporous Mesoporous Mater., 110136

Haynes, T., Bougnouch, O., Dubois, V., Hermans, S., 2020. Preparation of mesoporous silica nanocapsules with a high specific surface area by hard and soft dual templating approach: application to biomass valorization catalysis. Microporous Mesoporous Mater., 110400

Venezia, V., Sannino, F., Costantini, A., Silvestri, B., Cimino, S., Califano, V., 2020. Mesoporous silica nanoparticles for β-glucosidase immobilization by templating with a green material: tannic acid. Microporous Mesoporous Mater., 110203

Ke, J., Wang, Y., Wang, L., Yang, B., Gou, K., Qin, Y., Li, S., Li, H., 2020. Synthesis and characterization of core-shell mesoporous silica nanoparticles with various shell thickness as indomethacin carriers: in vitro and in vivo evaluation. Microporous Mesoporous Mater. 297, 110043.

Li, H., Zhao, Y., Liu, S., Li, P., Yuan, D., He, C., 2020. Hierarchical porous carbon monolith derived from lignin for high areal capacitance supercapacitors. Microporous Mesoporous Mater. 297, 109960.

Mishra, S., Rawal, A., Nebhani, L., 2020. Imprinting the location of an in-built RAFT agent and selective grafting of polymer chains inside or outside the pores of mesoporous silica nanoparticles. Microporous Mesoporous Mater. 294, 109898.

Chapa-González, C., Piñón-Urbina, A.L., García-Casillas, P.E., 2018. Synthesis of controlled-size silica nanoparticles from sodium metasilicate and the effect of the addition of PEG in the size distribution. Materials (Basel) 11 (4), 510.

Narayan, R., Nayak, U.Y., Raichur, A.M., Garg, S., 2018. Mesoporous silica nanoparticles: a comprehensive review on synthesis and recent advances. Pharmaceutics 10 (3), 118.

Shaikh, I.R., Shaikh, A.A., 2013. Utilization of wheat husk ash as silica source for the synthesis of MCM-41 type mesoporous silicates: a sustainable approach towards valorization of the agricultural waste stream. Res. J. Chem. Sci. ISSN 2231, 606X.

Renuka, N., Praveen, A., Anas, K., 2013. Influence of CTAB molar ratio in tuning the texture of rice husk silica into MCM 41 and SBA-16. Mater. Lett. 109, 70–73.

Espíndola-Gonzalez, A., Martínez-Hernández, A., Angeles-Chávez, C., Castano, V., Velasco-Santos, C., 2010. Novel crystalline SiO 2 nanoparticles via annelids bioprocessing of agro-industrial wastes. Nanoscale Res. Lett. 5 (9), 1408.

Kaliannan, D., Palaninaicker, S., Palanivel, V., Mahadeo, M.A., Ravindra, B.N., Jae-Jin, S., 2019. A novel approach to preparation of nano-adsorbent from agricultural wastes (Saccharum officinarum leaves) and its environmental application. Environ. Sci. Pollut. Res. 26 (6), 5305–5314.

Jang, H.T., Park, Y., Ko, Y.S., Lee, J.Y., Margandan, B., 2009. Highly siliceous MCM-48 from rice husk ash for CO_2 adsorption. Int. J. Greenhouse Gas Control 3 (5), 545–549.

Hu, X., Hao, X., Wu, Y., Zhang, J., Zhang, X., Wang, P.C., Zou, G., Liang, X.-J., 2013. Multifunctional hybrid silica nanoparticles for controlled doxorubicin loading and release with thermal and pH dual response. J. Mater. Chem. B 1 (8), 1109–1118.

Aryapour, H., Mahdavi, M., Mohebbi, S.R., Zali, M.R., Foroumadi, A., 2012. Anti-proliferative and apoptotic effects of the derivatives from 4-aryl-4H-chromene family on human leukemia K562 cells. Arch. Pharm. Res. 35 (9), 1573–1582.

La-Salvia, N., Lovón-Quintana, J.J., Lovón, A.S.P., Valença, G.P., 2017. Influence of aluminum addition in the framework of MCM-41 mesoporous molecular sieve synthesized by non-hydrothermal method in an alkali-free system. Mater. Res. 20 (6), 1461–1469.

Beygi, H., Karimi, E., Farazi, R., Ebrahimi, F., 2016. A statistical approach to synthesis of functionally modified silica nanoparticles. J. Alloys Compd. 654, 308–314.

Xu, H., Zhang, H., Wang, D., Wu, L., Liu, X., Jiao, Z., 2015. A facile route for rapid synthesis of hollow mesoporous silica nanoparticles as pH-responsive delivery carrier. J. Colloid Interface Sci. 451, 101–107.

Lenza, R.F., Vasconcelos, W.L., 2001. Structural evolution of silica sols modified with formamide. Mater. Res. 4 (3), 175–179.

Dabbaghian, M., Babalou, A., Hadi, P., Jannatdoust, E., 2010. A parametric study of the synthesis of silica nanoparticles via sol-gel precipitation method. Int. J. Nanosci. Nanotechnol. 6 (2), 104–113.

Thommes, M., Kaneko, K., Neimark, A.V., Olivier, J.P., Rodriguez-Reinoso, F., Rouquerol, J., Sing, K.S., 2015. Physisorption of gases, with special reference to the evaluation of surface area and pore size distribution (IUPAC Technical Report). Pure Appl. Chem. 87 (9–10), 1051–1069.

Sotomayor, F.J., Cychosz, K.A., Thommes, M., 2018. Characterization of micro/mesoporous materials by physisorption: concepts and case studies. Acc. Mater. Surf. Res. 3 (2), 36–37.

Kamba, S.A., Ismail, M., Hussein-Al-Ali, S.H., Ibrahim, T.A.T., Zakaria, Z.A.B., 2013. In vitro delivery and controlled release of doxorubicin for targeting osteosarcoma bone cancer. Molecules 18 (9), 10580–10598.

Bavnhøj, C.G., Knopp, M.M., Madsen, C.M., Löbmann, K., 2019. The role interplay between mesoporous silica pore volume and surface area and their effect on drug loading capacity. Int. J. Pharm. X 1, 100008.

Li, Z., Zhang, Y., Feng, N., 2019. Mesoporous silica nanoparticles: synthesis, classification, drug loading, pharmacokinetics, biocompatibility, and application in drug delivery. Expert Opin. Drug Deliv. 16 (3), 219–237.

Hu, X., Wei, W., Qi, X., Yu, H., Feng, L., Li, J., Wang, S., Zhang, J., Dong, W., 2015. Preparation and characterization of a novel pH-sensitive Salecan-g-poly (acrylic acid) hydrogel for controlled release of doxorubicin. J. Mater. Chem. B 3 (13), 2685–2697.

Limnell, T., Santos, H.A., Mäkilä, E., Heikkilä, T., Salonen, J., Murzin, D.Y., Kumar, N., Laaksonen, T., Peltonen, L., Hirvonen, J., 2011. Drug delivery formulations of ordered and nonordered mesoporous silica: comparison of three drug loading methods. J. Pharm. Sci. 100 (8), 3294–3306.

Naseri, M.H., Mahdavi, M., Davoodi, J., Tackallou, S.H., Goudarzvand, M., Neishabouri, S.H., 2015. Up regulation of Bax and down regulation of Bcl2 during 3-NC mediated apoptosis in human cancer cells. Cancer Cell Int. 15 (1), 55.